IRAQI JOURNAL OF APPLIED PHYSICS
Vol. 22, No. 3, July-September 2026, pp. 525-532

Seham H. Salman [1]
Israa A. Abbas [2]
Ali H.A. Alrazak [1]
Mohammed H. Mustafa [1]
Hind A. Mahdi [1]
Shaimaa A. Abbas [1*]

[1] Department of Physics, College of Education for Pure Science (Ibn-Alhaitham), University of Baghdad, Baghdad, IRAQ
[2] Department of Physics, College of Education, Mustansiriyah University, Baghdad, IRAQ
* Corresponding author email: shaimaa.a.a@ihcoedu.uobaghdad.edu.iq

Preparation of Nanostructured Co_3O_4 Thin Films Using Spray Technique for Gas Sensing Applications

Nanostructured thin films of cobalt oxide (Co_3O_4) were deposited on glass substrates using chemical spray pyrolysis at a substrate temperature of 673K. The deposited films were annealed at 773K for 60, 90, and 120 minutes to investigate their physical and gas sensing properties. X-ray diffraction results showed that the as-deposited films were amorphous, while the annealed films exhibited a polycrystalline cubic structure. The crystallite size increased from 51.74 to 55.33 nm with increasing annealing time. Microstrain and dislocation density were also evaluated. Atomic force microscopy analysis was used to examine the surface topography of the films. Optical properties were studied using UV-visible spectroscopy, revealing two direct band gaps: Eg_1 ranging from 1.98 to 2.09 eV and Eg_2 from 2.5 to 3.4 eV. Gas sensors fabricated from annealed and unannealed films showed improved sensitivity with operation temperature at 200°C for NO_2 and at 100°C for H_2S gases.

Keywords: Cobalt oxide; Nanostructures; Chemical spray pyrolysis; Gas sensors
Received: 22 February 2026; Revised: 26 April 2026; Accepted: 3 May 2026; Published: 1 July 2026

1. Introduction

Thin films of transparent conducting metal oxides (transparent conducting oxides – TCOs), such as In_2O_3, Co_3O_4, CdO, ZnO, and SnO_2, as well as tin oxide, have garnered significant attention due to their crucial role in the development of gas sensor devices. Because of their effective role in detecting environmental pollution caused by toxic, flammable, and hazardous gases that pose serious risks to human health, chemical gas sensors hold great significance in modern sensing applications. Among the most notable gases are CO, CO_2, CH_4, H_2, NH_3, H_2S, NO_2, and SO_2, in addition to alcohols such as methanol (CH_3OH) and ethanol, as well as volatile organic compounds (VOCs) [1-6], all of which represent a direct threat to human life.

Cobalt oxide (Co_3O_4) is characterized by an indirect energy gap in the range of 1.6-2.2 eV [7] and is classified as a p-type semiconductor. In indirect electronic transitions, electrons move between the conduction and the valence band with the assistance of phonons to satisfy the conservation laws of energy and momentum. For these properties, Co_3O_4 is, in principle, a suitable material for gas sensing applications, as the sensing process is associated with thermal changes. The sensitivity of cobalt oxide increases with temperature until it reaches an optimum value due to increased oxygen uptake and activation of surface reactions [8].

Cobalt oxide is one of the semiconducting materials that has received significant. This material has attracted significant attention due to its unique physical and chemical properties. It presents antiferromagnetic behavior and contains two types of energy band gaps. Moreover, its distinguished by its high efficiency and excellent chemical stability, making it an important material for photovoltaic (PV) applications [9-12].

Co_3O_4 has a face-centered cubic (FCC) crystal structure, in which Co^{2+} ions occupy the tetrahedral sites (8a) and Co^{3+} ions reside in the octahedral sites (16d). In contrast, oxygen ions are positioned within the face-centered cubic lattice (32e sites) [13]. Co_3O_4 is involved in many electro-optical applications, such as the selective absorption of solar energy in solar cells, lithium batteries, supercapacitors, and gas sensors, in addition to its applications in biomedical fields and pharmacology.

In this study, a gas sensor based on pure Co_3O_4 was fabricated, and its sensing properties were systematically investigated [14,15].

2. Experimental Part

Cobalt (III) oxide (Co_3O_4) nanostructured films were prepared using spray pyrolysis on clean glass substrates. Cobalt nitrate hexahydrate, with a purity of 97.5% (Oxford Laboratory Chemicals), was used as a precursor to prepare Co_3O_4 films at a molar concentration of 0.06 M. The molar concentration of the saline solution and the mass of the salt used were calculated using the relationship [14,15]:

$$M = \frac{W_t}{M_{wt}} \frac{1000}{V} \quad (1)$$

where M is the molar concentration (mol/L), W_t is the mass of solute (g), and M_{wt} is the molar mass

The precursor was made at room temperature; 0.1746 g cobalt nitrate hexahydrate was dissolved in 10

mL of distilled water. The resulting solution was then continuously stirred for 30 minutes. The glass substrate was cleaned in a series in an ultrasonic cleaner using ethanol for 15 minutes, then rinsed with deionized water for 15 minutes to eliminate contaminants. Subsequently, the substrates were heated at 673 K. The distance between the spray nozzle and the glass substrate was maintained at 24 cm. The spraying process took 3 s, followed by a 57 s pause to allow the base to return to its desired temperature. The spraying process included 12 cycles, spray rate of 0.166 ml/s and air pressure of 10^5 Pa. Finally, the prepared samples were annealed at 773 K for 60, 90, and 120 minutes using a KSL-1100 X furnace. After the power was switched off, the annealed samples were left within the furnace for the entire night.

The thickness of the prepared thin films was determined using optical interferometry with a He-Ne laser at a wavelength of 0.632 μm. The film thickness (d) was calculated by the following equation [16]:

$$d = \frac{\Delta x}{x}\frac{\lambda}{2} \quad (2)$$

where x is the bright fringe width, Δx is the distance between two adjacent fringes, and λ is the wavelength of the He-Ne laser

Using PHILIPS X-ray diffractometer, the X-ray diffraction (XRD) patterns were employed to determine the crystalline structure of the Co_3O_4 films. A SHIMADZU UV-visible spectrophotometer was used to study optical properties of the prepared films. Surface topography was examined using atomic force microscope (AFM). To fabricate the gas sensor to detect gases (NO_2 and H_2S), aluminum electrodes were thermally evaporated onto the sample surface in a comb pattern. The wires were then connected using a silver paste. Test gases were detected as the sample was placed in a locally manufactured chamber. The gas sensor readings were taken at different operating temperatures.

3. Results and Discussion

Figure (1) illustrates three peaks, which correspond to cobalt oxide (220), (311), and (440). This indicates that the prepared thin films are polycrystalline with cubic phase. The obtained results are in conformity with the standard ICDD card (00-037-0630). It is evident from Fig. (1) that the reflection sharpness and intensity increase with increasing annealing times due to elevated annealing time supplying energy to the crystallites graining, sufficient energy to occupy proper equilibrium sites, leading to enhanced crystallinity and better film orientation. This is consistent with the study [16]. The XRD results of the Co_3O_4 films are displayed in table (1).

The crystallite size (D) was calculated for three peaks using the following equation for thin films [18-20]:

$$D = \frac{0.9\lambda}{\beta cos\theta} \quad (3)$$

Here, β represents the full-width at half maximum (FWHM)

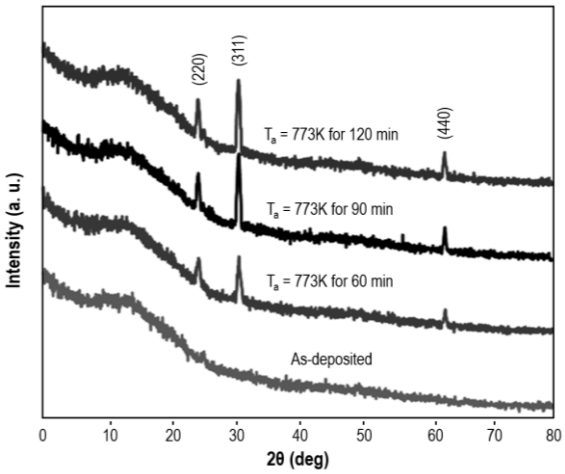

Fig. (1) XRD patterns of Co_3O_4 thin films with various annealing times

The micro-strain (ε) and the density of dislocation (δ) were determined by following equations [21-24]:

$$\delta = \frac{1}{D^2} \quad (4)$$

$$\varepsilon = \frac{\beta cos\theta}{4} \quad (5)$$

Table (1) shows the effect of annealing time (60, 90, and 120 minutes) on the structural properties extracted from XRD. We note that the crystallite size (D) increases from 63.346 to 67.884 nm with increasing annealing time for the (220) direction, from 51.74 to 55.334 nm for the (311) direction, and from 48.768 to 52.94 nm for the (400) direction. This is due to grain growth and improved crystallinity resulting from increased energy for atomic utilization. When the average crystallite size for all directions was taken for each time, the pore size also increased from 54.619 to 58.721 nm. Conversely, the dislocation density (δ) decreased from ≈4.2 to 3.57×10^{14} lines/m² due to its inverse relationship with grain size, according to Eq. (5) indicating a decrease in crystal defects and an improvement in structural quality. A decrease in microstress (ε) was also observed with increasing annealing time, indicating relaxation of internal stresses following the arrangement of atoms within the crystal lattice. Furthermore, the convergence of d-spacing values with standard values and the slight offset at the 2θ angles indicate improved regularity of the crystal lattice, while the constant evolution along the (220), (311), and (440) directions remained unchanged [25].

Figures (2) to (5) and table (2) show that the pre-annealed sample had a high average grain diameter of 80.34 nm with moderate surface roughness, resulting from agglomeration and surface irregularity. During annealing for 60 minutes, the grain diameter decreased significantly due to the breakdown of these agglomerates and the onset of recrystallization. At 90

minutes, it increased due to the dominance of grain growth driven by atomic diffusion. Finally, at 120 minutes, the grain size decreased again, accompanied by a marked improvement in surface smoothness, attributed to the reorganization of the surface structure and increased homogeneity. This behavior is consistent with recent studies of Co_3O_4 films that indicate a balance between nucleation and granulation processes during annealing [26].

Table (2) The AFM parameters

Annealing Time (min)	Mean Diameter (nm)	Roughness (nm)	R.M.S. (nm)
As deposited	80.34	18.99	37.44
60	37.46	35.33	72.45
90	67.12	31.62	70.36
120	59.12	6.99	9.73

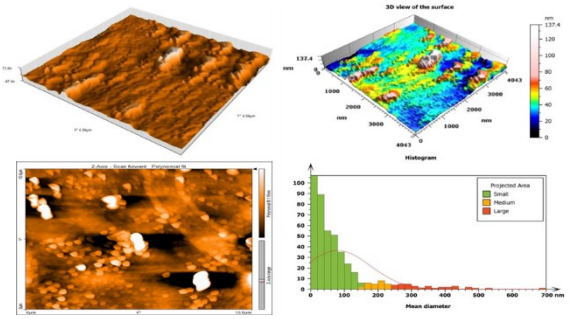

Fig. (2) AFM results for the un-annealed Co_3O_4 thin film

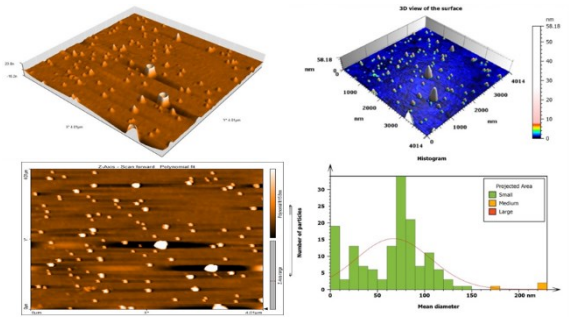

Fig. (3) AFM results for Co_3O_4 thin film annealed for 60 min.

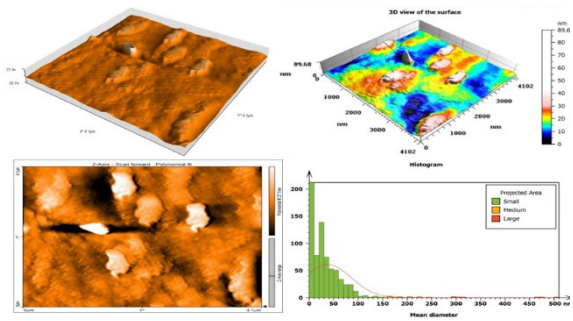

Fig. (4) AFM results for Co_3O_4 thin film annealed for 60 min.

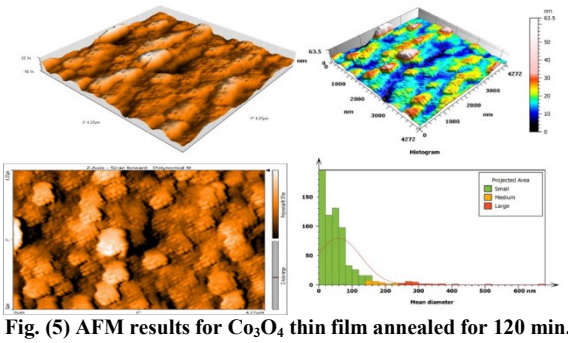

Fig. (5) AFM results for Co_3O_4 thin film annealed for 120 min.

The optical characteristics of the prepared Co_3O_4 films, including the transmittance, were determined in the spectral range of 300-1100 nm. Figure (6) shows the transmittance of the as-deposited Co_3O_4 films heat-treated for different times. It can be seen that the transmittance improves with increasing annealing time. This increase in transmittance can be explained by the relatively better crystallinity of the annealed films. Figure (6) also shows two sharp absorption edges.

The energy band gap (E_g) of the Co_3O_4 films was determined from the transmittance using Tauc's method as [27-29]

$$(\alpha h\nu)^2 = A\left(h\nu - E_g\right) \qquad (6)$$

where A is a constant. The energy band gap (E_g) was calculated by extrapolating the linear region of the curve to the hυ axis

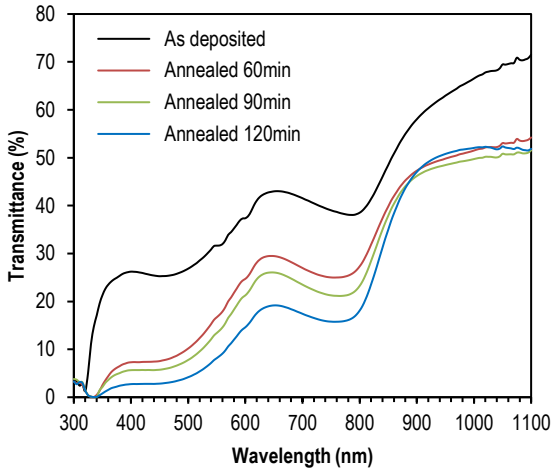

Fig. (6) Transmission spectra of Co_3O_4 thin films before and after annealing

The Co_3O_4 thin films show two direct band gaps, which are in good consistency with reference [30]. Two distinct E_g values are extracted because, in optical measurements (UV-visible), two absorption edges often appear, since absorption does not represent just one "valence→conduction" transition, but rather the sum of charge-transfer transitions associated with both Co^{2+} and Co^{3+} [31]. E_{g2} decreased with increasing annealing time as different oxidation states of cobalt ions and surface defects play a key role in modifying

the electronic structure of Co_3O_4, which explains the observed changes in the band gap energy of Co_3O_4 thin films. These findings were confirmed by the study of Bessinger et al. [32]. The first energy gap increases after annealing time of 60 min and then decreases with increasing annealing time, which is attributed to improved crystallinity and reduced defect levels. This leads to a reduction in the quantum confinement effect.

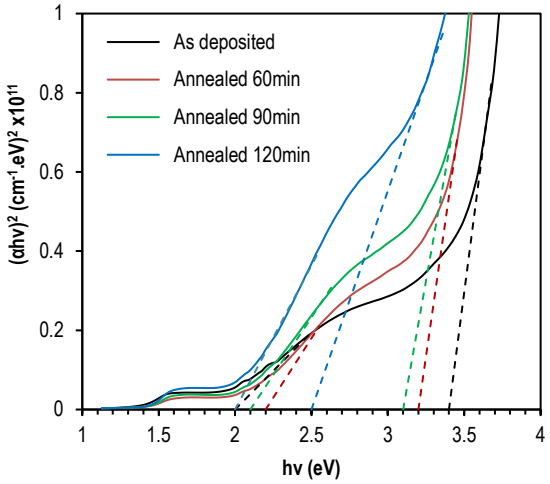

Fig. (7) $(\alpha h\upsilon)^2$ vs. photon energy for Co_3O_4 thin films; as-deposited, and annealed at 773K with different annealing times

Table (3) The energy gap values of Co_3O_4

Sample	Eg_1	Eg_2
As-deposited	2	3.4
60	2.15	3.2
90	2.1	3.05
120	2	2.5

The consistency between the XRD patterns and UV-visible results confirms that grain size control and crystalline structure optimization are key factors in adjusting the bandgap energy and electronic properties of nanostructured Co_3O_4 thin films.

The sensing mechanism in Co_3O_4 thin films relies on the adsorption of oxygen onto the surface and the formation of active ionic species such as O^-. When the film is exposed to a reducing gas such as H_2S, it reacts with the adsorbed oxygen according to the following reaction:

$H_2O_2 + O^- \rightarrow H_2O_2 + S_2O_2 + e^-$

This leads to release electrons and a decrease in hole concentration, thus increasing resistance. When exposed to an oxidizing gas such as NO_2, it is adsorbed onto the surface and attracts electrons according to the following reaction:

$NO_2 + e^- \rightarrow NO_2$

This leads to an increase in hole concentration and a decrease in resistance. Therefore, the sensor's behavior depends on the nature of the gas (reducing or oxidizing) and the type of semiconductor (p-type or n-type), and Co_3O_4 is a p-type semiconductor. The sensor was investigated before and after annealing to (NO_2 and H_2S) at different operating temperatures (RT, 100, 200°C). The sensitivity of Co_3O_4 thin films for NO_2 gas by [30, 33-35]

$$S = \frac{R_a - R_g}{R_g} \times 100\% \quad (7)$$

where R_a and R_g are the resistance of the Co_3O_4 thin films in air and in presence of gas, respectively

Figure (8) and table (4) show that the sensitivity of the Co_3O_4 thin film sensor increases with increasing operating temperature for all models, rising from low values at room temperature to a maximum at 200°C. This is attributed to the activation of chemisorption of NO_2 gas and increased surface reactivity, leading to the removal of more electrons and an increase in hole concentration, thus reducing resistance and increasing sensitivity [36]. Optimal performance was observed at a preparation time of 60 minutes, resulting in the highest sensitivity (17.355%), indicating that the surface structure is more favorable at this time (larger surface area and more effective sites). Sensitivity decreases at 90 and 120 minutes due to particle growth or agglomeration, which reduces the effective surface area and the number of adsorption sites [37]. The response time improves (decreases) with increasing temperature up to approximately 100°C due to the accelerated reaction, while at 200°C it fluctuates due to the balance between adsorption and decomposition. Recovery time improves at higher temperatures due to accelerated gas removal from the surface [38]. The sensitivity of Co_3O_4 thin films for H_2S was estimated by [39-41]:

$$S = \frac{R_g - R_a}{R_a} \times 100\% \quad (8)$$

Table (4) Parameters of Co_3O_4 thin film gas sensor for NO_2 gas at different operating temperatures

Sample	Operating Temperature (°C)	Sensitivity (%)	Response time (s)	Recovery time (s)
As deposited	RT	0.208	28.8	57.6
	100	3.832	26.1	61.2
	200	5.061	24.3	44.1
60 min	RT	1.857	27.9	83.7
	100	10.633	18.9	63.9
	200	17.355	24.3	62.1
90 min	RT	0.519	29.7	87.3
	100	6.926	23.4	89.1
	200	10.023	27	60.3
120 min	RT	0.796	22.5	89.1
	100	2.404	23.4	63
	200	4.283	30.6	59.4

Figure (9) shows the results obtained from table (5). The Co_3O_4 thin films sensor for H_2S gas has an optimal operating temperature (≈100°C), where equilibrium between adsorption and surface reaction is achieved. At 200°C, the sensitivity decreases due to de-adsorption. The highest sensitivity was recorded at 100°C for the sample annealed for 90 min (18.78%) because the optimal surface structure is achieved at this time [37].

The response time decreases with increasing temperature (reaching 13.5 s at 200°C) due to the accelerated reaction. The recovery time improves at higher temperatures due to the accelerated removal of gas from the surface [36].

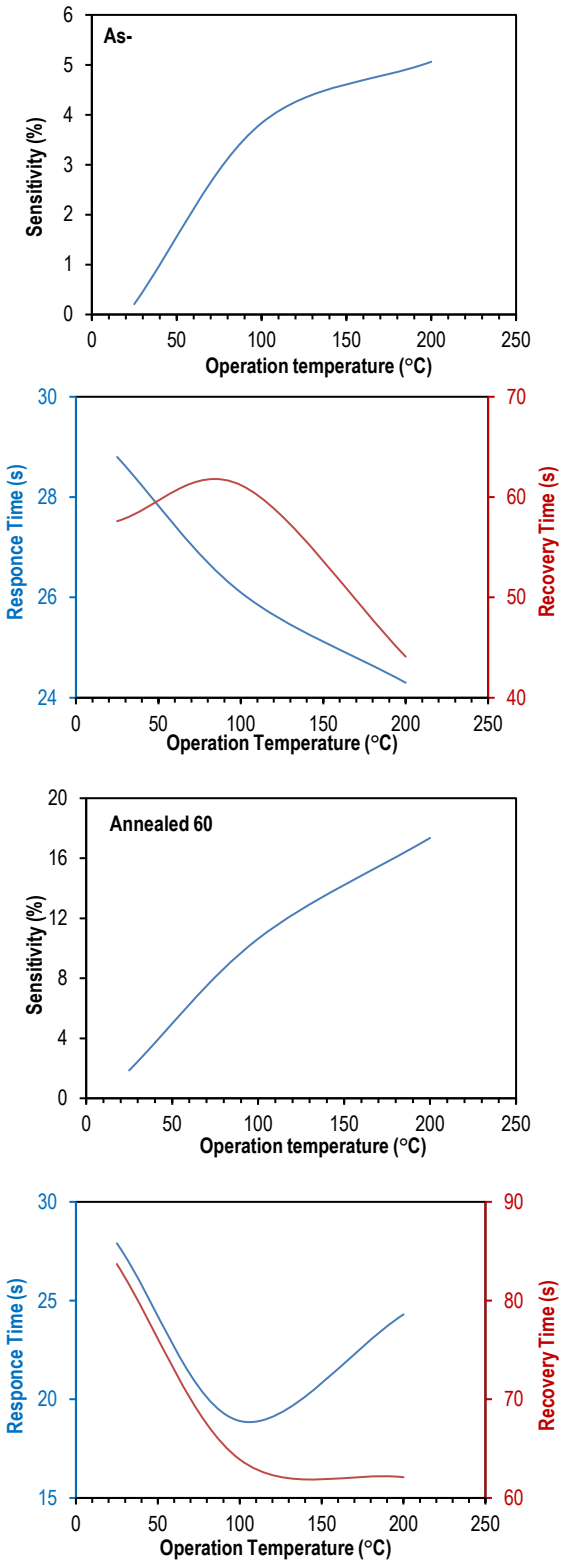

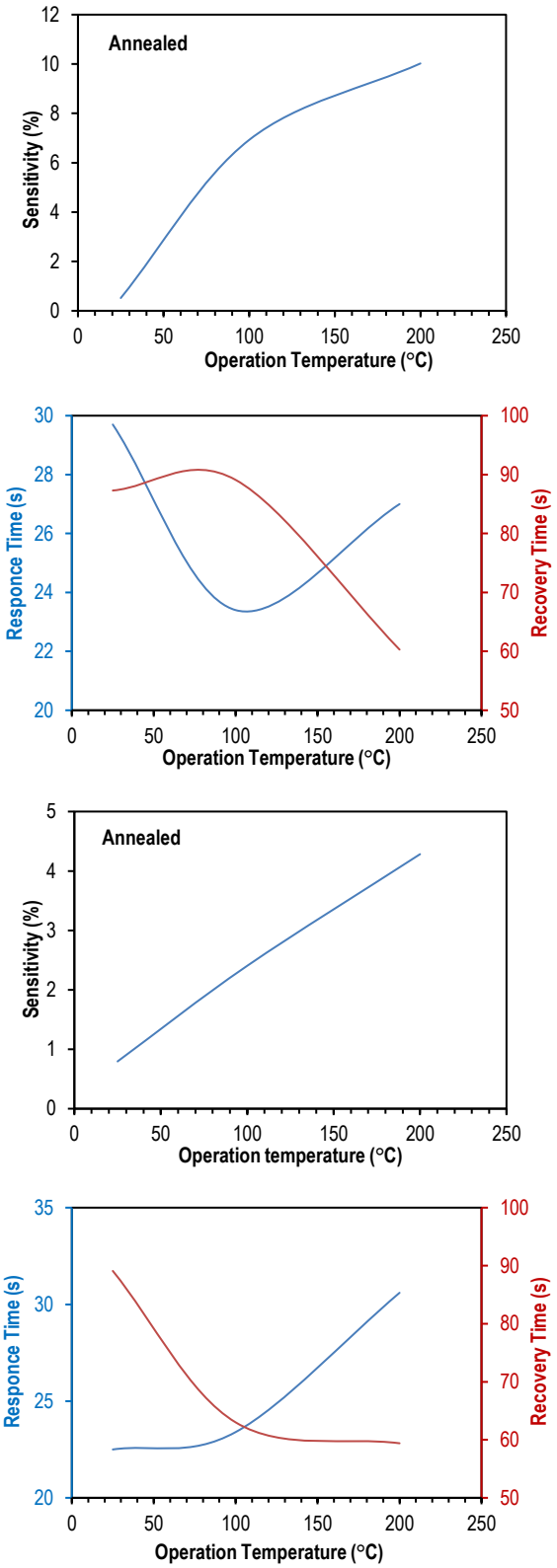

Fig. (8) Variation of sensitivity, response and recovery times of Co_3O_4 thin films for NO_2 gas at different working temperatures

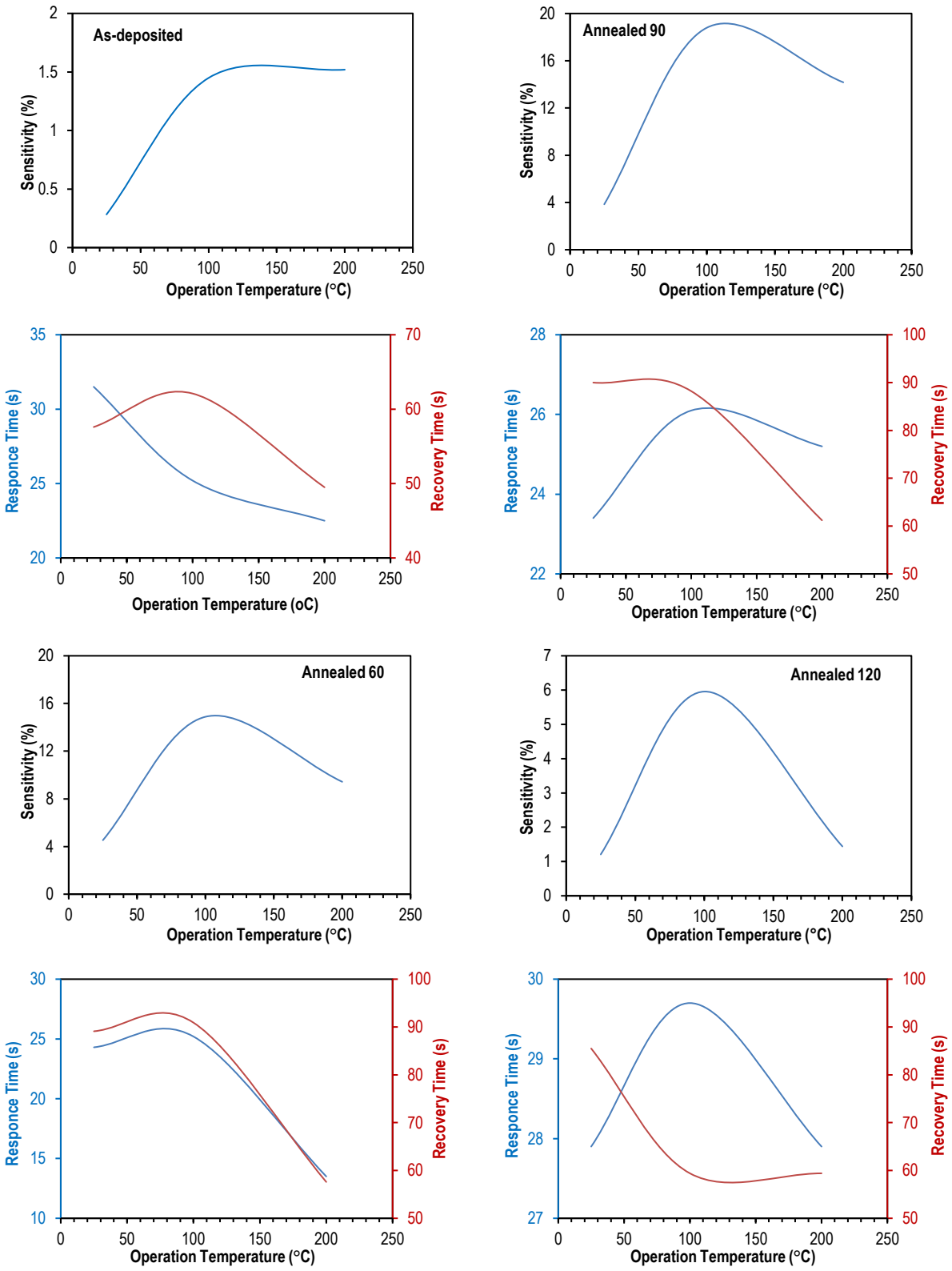

Fig. (9) Variation of sensitivity, response and recovery times of Co_3O_4 thin films for H_2S gas at different working temperatures

Table (5) Parameters of Co_3O_4 thin film gas sensor for H_2S gas at different operating temperatures

Sample	Operating Temperature (°C)	Sensitivity (%)	Response time (s)	Recovery time (s)
As deposited	RT	0.283	31.5	57.6
	100	1.449	25.2	62.1
	200	1.519	22.5	49.5
60 min	RT	4.528	23.4	90
	100	14.882	26.1	88.2
	200	9.428	25.2	61.2
90 min	RT	3.848	24.3	89.1
	100	18.7898	25.2	90.9
	200	14.171	13.5	57.6
120 min	RT	1.207	27.9	85.5
	100	5.957	29.7	59.4
	200	1.441	27.9	59.4

4. Conclusions

Co_3O_4 thin films were deposited at 400°C and annealed at 500°C for different times. The Co_3O_4 thin films have nanostructures and polycrystalline structure with cubic phase after annealing. The preferential orientation is around (311). The crystallinity improves with annealing time. Therefore, these films can be used for gas sensing applications. The annealing led to a decrease in transmittance and an increase in absorbance. The prepared thin films have two energy gaps due to two absorption edges often appearing since the absorption represents the sum of charge-transfer transitions associated with both Co^{2+} and Co^{3+}. Gas sensitivity was at maximum for Co_3O_4 thin films annealed for 60 min for NO_2 and H_2S gases, and the sensitivity increases with operating temperature.

References

[1] J. Wang et al., "Room-temperature gas sensors based on ZnO nanorod/Au hybrids: Visible-light-modulated dual selectivity to NO_2 and NH_3", *J. Hazard. Mater.*, 381 (2020) 120919.

[2] J. Chao et al., "Facile fabrication of ZnO/C nanoporous fibers and ZnO hollow spheres for high performance gas sensor", *Sens. Actuat. B: Chem.*, 298 (2019) 126927.

[3] T. Hsueh, C. Peng and W. Chen, "A transparent ZnO nanowire MEMS gas sensor prepared by an ITO micro-heater", *Sens. Actuat. B: Chem.*, 304 (2020) 127319.

[4] S.P. Choudhury et al., "BN quantum dots decorated ZnO nanoplates sensor for enhanced detection of BTEX gases", *J. Alloys Compd.*, 815 (2020) 152376.

[5] P. Cao et al., "Ethanol sensing behavior of Pd-nanoparticles decorated ZnO nanorod based chemiresistive gas sensors", *Sens. Actuat. B: Chem.*, 298 (2019) 126850.

[6] V.S. Bhati, M. Hojamberdiev and M. Kumar, "Enhanced sensing performance of ZnO nanostructures-based gas sensors: A review", *Energy Rep.*, 6 (2020) 46–62.

[7] S.H. Sabeh and R.J. Abd Al-Hassan, "Structural, morphological and optical properties of Co_3O_4 thin film", *Eng. Technol. J.*, 34(4) (2016) 553–559.

[8] J. Wöllenstein et al., "Cobalt oxide based gas sensors on silicon substrate for operation at low temperatures", *Sens. Actuat. B: Chem.*, 93(1-3) (2003) 442–448.

[9] A. Lakehal et al., "Structural, optical and electrical properties of Ni-doped Co_3O_4 prepared via sol-gel technique", *Mater. Res.*, 21(3) (2018) e20170545.

[10] W. Daranfed, N. Guermat and K. Mirouh, "Experimental study of precursor concentration of Co_3O_4 thin films used as solar absorbers", *Ann. Chim. Sci. Mater.*, 44(2) (2020) 121–126.

[11] N.A.H. Hashim and F.J. Kadhim, "Structural and Optical Characteristics of Co_3O_4 Nanostructures Prepared by DC Reactive Magnetron Sputtering", *Iraqi J. Appl. Phys.*, 18(4) (2022) 31-36.

[12] N.A.H. Hashim, F.J. Kadhim and Z.S. Abdulsattar, "Characterization of Electrochromism and Photoelectrochromism of N-Doped TiO_2 and Co_3O_4 Thin Films Prepared by DC Reactive Magnetron Sputtering: Comparative Study", *Iraqi J. Appl. Phys.*, 19(1) (2023) 5-12.

[13] R. Obodo et al., "Influence of pH and annealing on the optical and electrochemical properties of Co_3O_4 thin films", *Surf. Interfaces*, 16 (2019) 114–119.

[14] S.I. Maki and A.I. Hassan, "Structure and optical properties of copper-doped cobalt oxide thin films prepared by spray pyrolysis", *Int. J. Eng. Sci. Res. Technol.*, 6(3) (2017) 527–535.

[15] S. Iqbal et al., "Effect of sintering temperature on the structure, morphology and optical properties of Co_3O_4 nanocrystalline materials", *J. Photochem. Photobiol. A Chem.*, 386 (2020) 112130.

[16] R.M. Aljarrah and A.M. Aljawdah, "Concentration effects on characteristics of gas sensors based on SnO_2:Sb_2O_3 thin films", *Mater. Sci. Forum*, 1039 (2021) 416-425.

[17] M.H. Mustafa and A.A. Shihab, "Influence of heat treatment on the efficiency of WO_3:Au NPs optoelectronic device prepared by spray pyrolysis technique", *J. Theor. Appl. Phys.*, Special Issue (2024) article 7.

[18] L. Chopra, **"Thin Film Phenomena"**, Academic Press (1969).

[19] M. Abdel Rafea, A. Eid and N. Mustapha, "The effect of annealing on the structure, morphology and optical properties of Co_3O_4 thin films prepared using a modified dip coating technique", *Mater. Sci. Eng. B*, 290 (2023) 116294.

[20] A. Hazem and M.H. Mustafa, "Influence of silver doping on the properties of sprayed cadmium telluride films", *J. Phys. Conf. Ser.*, 3028(1) (2025) 012048.

[21] S.H. Salman, N.A. Hassan and G.S. Ahmed, "Copper telluride thin films for gas sensing applications", *Chalcogen. Lett.*, 19(2) (2022) 125-130.

[22] R. Saad et al., "Enhanced carbon dioxide sensing performance of doped cobalt oxide thin films", *RSC Adv.*, 14(49) (2024) 36852-36867.

[23] H.I. Mohammed et al., "I-V characteristics of polycrystalline CAZTSe heterojunction solar cells", *Int. J. Nanoelectron. Mater.*, 16(4) (2024) 749-758.
[24] M.H. Mustafa et al., "Influence of annealing on the optoelectronic properties of sprayed p-NiO/n-CdS", *J. Mater. Sci. Mater. Electron.*, 35(22) (2024) 1535.
[25] M.H. Mustafa and A.A. Shihab, "Effect of ratio gold nanoparticles on the properties of amorphous tungsten trioxide thin films", *J. Ovonic Res.*, 19(6) (2023) 623-630.
[26] I.A. Abbas and S.Q. Hazaa, "Influence of annealing on the structural, morphology and optical properties of TiO_2 thin films", *AIP Conf. Proc.*, 2307 (2020) 020037.
[27] C. Suryanarayana, **"Equipment for mechanical alloying"**, in **Mechanical Alloying and Milling**, 1st ed., CRC Press (2004), pp. 35-58.
[28] C.H. Scharf et al., "Role of defects in reversible surface restructuring and activity of Co_3O_4 oxygen evolution electrocatalysts", *ACS Catal.*, 16(5) (2026) 4877-4891.
[29] S.H. Salman et al., "Effect of annealing time on physical properties of TiO_2 thin films", *Iraqi J. Appl. Phys.*, 20(1A) (2024) 37-42.
[30] D. Hadi, H. Hadi and S. H. Salman, "Effect of annealing on the physical characteristics of In_2O_3 nanoparticle films", *Ann. Chim. Sci. Mater.*, 49(3) (2025) 315-320.
[31] S.H. Salman, S.M. Ali and G.S. Ahmed, "Effect of annealing on structural and optical properties of InSe thin films", *J. Phys. Conf. Ser.*, 1879(3) (2021) 032058.
[32] A. Louardi et al., "Effect of annealing treatment on Co_3O_4 thin films properties prepared by spray pyrolysis", *J. Mater. Environ. Sci.*, 8(2) (2017) 485-493.
[33] K.S. Gabriel's et al., "Electrical and optical properties of cobalt oxide thin films prepared by ion-beam sputtering", *Tech. Phys.*, 68(S3) (2023) S430-S436.
[34] M.C. Biesinger et al., "Resolving surface chemical states in XPS analysis of first row transition metals, oxides and hydroxides: Cr, Mn, Fe, Co and Ni", *Appl. Surf. Sci.*, 257(7) (2011) 2717-2730.
[35] I.A. Abbas, S.Q. Hazaa and S.H. Salman, "Employment of titanium dioxide thin film on NO_2 gas sensing", *J. Phys.: Conf. Ser.*, 1879(3) (2021) 032061.
[36] A.S. Garde, "Humidity sensing properties of WO_3 thick film resistor prepared by screen printing technique", *J. Alloys Compd.*, 617 (2014) 367-373.
[37] S.H. Salman, A.A. Shihab and A.H.Kh. Elttayef, "Design and construction of nanostructure TiO_2 thin film gas sensor prepared by R.F magnetron sputtering technique", *Energy Procedia*, 157 (2019) 283-289.
[38] A. Tamvakos et al., "NO_2 gas sensing mechanism of ZnO thin-film transducers: Physical experiment and theoretical correlation study", *ACS Sens.*, 1(4) (2016) 406-412.
[39] G. Korotcenkov, **"Handbook of gas sensor materials: Properties, advantages and shortcomings for applications"**, vol. 1: Conventional approaches, Springer (2013).
[40] S. Basu and P. Bhattacharyya, "Recent developments on graphene and graphene oxide based solid state gas sensors", *Sens. Actuators B Chem.*, 173 (2012) 1-21.
[41] M.H. Faisal and S.H. Salman, "Effect of oxidation times on gas sensitivity and characterization for In_2O_3 thin films produced by thermal evaporation", *J. Phys.: Conf. Ser.*, 2857(1) (2024) 012010.
[42] S.H. Salman et al., "Ammonia gas sensing using porous silicon", *J. Phys.: Conf. Ser.*, 2857(1) (2024) 012051.
[43] A.H. Alrazak et al., "Influence of doping with silver nanoparticles on molybdenum oxide thin films", *Digest J. Nanomater. Biostruct.*, 20(1) (2025) 191-199.

Table (1) Structural characteristics of Co_3O_4 thin films

Annealing Time (min)	$2\theta_{XRD}$	$2\theta_{std}$	Crystallite Size (D) (nm)	$\delta \times 10^{14}$ (line/m^2)	Stress (ε) *10^{-3}	d-spacing (Å)$_{XRD}$	d-spacing (Å)$_{std}$	(hkl)
60	31.373	31.272	63.346	2.49	0.57	2.849	2.858	(220)
	36.934	36.853	51.742	3.74	0.699	2.432	2.437	(311)
	65.309	65.238	48.768	4.2	0.74	1.428	1.429	(440)
90	31.339		66.009	2.3	0.55	2.852		
	36.901		54.308	3.39	0.67	2.434		
	65.275		51.033	3.84	0.71	1.428		
120	31.306		67.824	2.17	0.53	2.855		
	36.867		55.334	3.27	0.65	2.436		
	65.242		52.944	3.57	0.68	1.429		

